Differential Interactions of Na^+ Channel Toxins with T-type Ca^{2+} Channels

Hui Sun,[1] Diego Varela,[4] Denis Chartier,[2] Peter C. Ruben,[3] Stanley Nattel,[2] Gerald W. Zamponi,[4] and Normand Leblanc[5]

[1]Excigen, Inc., Baltimore, MD 21224
[2]Department of Medicine, Université de Montréal, and Research Centre, Montréal Heart Institute, Montréal, Québec, Canada
[3]School of Kinesiology, Faculty of Applied Sciences, Simon Fraser University, Vancouver, British Columbia, Canada V6B 5K3
[4]Department of Physiology and Biophysics, Hotchkiss Brain Institute, University of Calgary, Calgary, Alberta, Canada T2N 1N4
[5]Department of Pharmacology, Center of Biomedical Research Excellence (COBRE), University of Nevada School of Medicine, Reno, NV 89557

Two types of voltage-dependent Ca^{2+} channels have been identified in heart: high (I_{CaL}) and low (I_{CaT}) voltage-activated Ca^{2+} channels. In guinea pig ventricular myocytes, low voltage–activated inward current consists of I_{CaT} and a tetrodotoxin (TTX)-sensitive I_{Ca} component ($I_{Ca(TTX)}$). In this study, we reexamined the nature of low-threshold I_{Ca} in dog atrium, as well as whether it is affected by Na^+ channel toxins. Ca^{2+} currents were recorded using the whole-cell patch clamp technique. In the absence of external Na^+, a transient inward current activated near −50 mV, peaked at −30 mV, and reversed around +40 mV (HP = −90 mV). It was unaffected by 30 µM TTX or micromolar concentrations of external Na^+, but was inhibited by 50 µM Ni^{2+} (by ∼90%) or 5 µM mibefradil (by ∼50%), consistent with the reported properties of I_{CaT}. Addition of 30 µM TTX in the presence of Ni^{2+} increased the current approximately fourfold (41% of control), and shifted the dose–response curve of Ni^{2+} block to the right (IC_{50} from 7.6 to 30 µM). Saxitoxin (STX) at 1 µM abolished the current left in 50 µM Ni^{2+}. In the absence of Ni^{2+}, STX potently blocked I_{CaT} (EC_{50} = 185 nM) and modestly reduced I_{CaL} (EC_{50} = 1.6 µM). While TTX produced no direct effect on I_{CaT} elicited by expression of $hCa_V3.1$ and $hCa_V3.2$ in HEK-293 cells, it significantly attenuated the block of this current by Ni^{2+} (IC_{50} increased to 550 µM Ni^{2+} for $Ca_V3.1$ and 15 µM Ni^{2+} for $Ca_V3.2$); in contrast, 30 µM TTX directly inhibited $hCa_V3.3$-induced I_{CaT} and the addition of 750 µM Ni^{2+} to the TTX-containing medium led to greater block of the current that was not significantly different than that produced by Ni^{2+} alone. 1 µM STX directly inhibited $Ca_V3.1$-, $Ca_V3.2$-, and $Ca_V3.3$-mediated I_{CaT} but did not enhance the ability of Ni^{2+} to block these currents. These findings provide important new implications for our understanding of structure–function relationships of I_{CaT} in heart, and further extend the hypothesis of a parallel evolution of Na^+ and Ca^{2+} channels from an ancestor with common structural motifs.

The Journal of General Physiology

INTRODUCTION

Voltage-gated Na^+ and Ca^{2+} channels are ubiquitously expressed in excitable cells across the animal kingdom and from an evolutionary standpoint have been proposed to have arisen from a common ancestor, primarily by gene duplication (Strong and Gutman, 1993; Hille, 2001). The pore-forming or α-subunit of Na^+ and Ca^{2+} channels share in common the basic structure of a single linear sequence of amino acids characterized by four repeat sequences containing each six transmembrane domains (S1–S6), with the fourth transmembrane segment of each repeat bearing positively charged residues conferring voltage-sensitive properties to the channel. For both classes of channels, the amino acid segment between S5 and S6 of each repeat dips back into the membrane from the extracellular space and forms the basic structure of the pore or P-loop of the channel. Each P-loop repeat shares one critical residue that forms a ring of four amino acid residues conferring ion selectivity and permeation across the pore. For Na^+ channels, the signature sequence of repeats I–IV is DEKA (Catterall, 2000), whereas for Ca^{2+} channels, it is EEXX (Perez-Reyes, 2003), where X is either E or D (Fig. 1; SF, selectivity filter). Mutation of the Lys of repeat III or Ala of repeat IV to Glu conferred Ca^{2+} and Ba^{2+} selectivity to Na^+ channels, again supporting commonality in their evolutionary heritage (Heinemann et al., 1992).

Among the three subfamilies of Ca^{2+} channels encoded by the Ca_V genes (Ca_V1, Ca_V2, and Ca_V3), the Ca_v3 subfamily encoding low threshold voltage-activated Ca^{2+} channels commonly referred to as T-type (for "transient"; I_{CaT}) Ca^{2+} channels has been hypothesized to be the closest Ca^{2+} channel subfamily to the Na^+ channel

Correspondence to Normand Leblanc: nleblanc@medicine.nevada.edu
H. Sun and D. Varela contributed equally to this paper.
The online version of this article contains supplemental material.

Abbreviations used in this paper: HP, holding potential; LVA, low voltage–activated inward Ca^{2+} current; SF, selectivity filter; STX, saxitoxin; TTX, tetrodotoxin.

The Rockefeller University Press $30.00
J. Gen. Physiol. Vol. 132 No. 1 101–113
www.jgp.org/cgi/doi/10.1085/jgp.200709883

Figure 1. Amino acid sequence alignments of the pore region of several vertebrate voltage-gated Na^+ and Ca^{2+} channels. This figure shows the alignments of P-loop residues located between transmembrane segments S5 and S6 of the four domains (Domains I–IV) of four mammalian ($Na_V1.4$, $Na_V1.5$, $Na_V1.8$, and $Na_V1.9$) and one garter snake ($tsNa_V1.4$; from Sonoma County, CA), Na^+ channel genes, and three mammalian T-type ($Ca_V3.1$, $Ca_V3.2$, and $Ca_V3.3$), and one L-type Ca^{2+} channel ($Ca_V1.2$) gene. These sequences were imported from the GenBank/EMBL/DDBJ (http://www.ncbi.nlm.nih.gov) with the accession no. (Access #) for each protein indicated to the right. Small numbers before and after the sequences indicate the absolute position (P) of the first and last amino acids from the N terminus of the translated protein. Overlaid are also shown relative positions before or after the selectivity filter (SF; 0) in each domain. These sequences were aligned using Vector NTI Advance (v. 8.0, InforMax). Please note that only predicted sequences were available for the canine Na^+ and Ca^{2+} channel genes but those were identical to their corresponding human sequences. Residues highlighted in dark green indicate identical residues, those in light green indicate equivalent substitutions based on a Blosum Matrix 45 score ≥1, those shaded in red indicate residues found to play a role in TTX and STX binding, and those highlighted in pink are Ca^{2+} channel residues that differ from residues involved in TTX and STX binding.

genes (Hille, 2001). Similar to Na^+ channels and contrary to high threshold voltage-gated Ca^{2+} channels (e.g., L-type), T-type Ca^{2+} channels activate in the negative range of membrane potentials and exhibit relatively fast activation and inactivation kinetics and have a small unitary conductance (~7 pS with 100 mM Ca^{2+} or Ba^{2+} as charge carrier). There is also recent evidence for similarities in the pore region between Na^+ channels and T-type Ca^{2+} channels. McNulty et al. (2006) recently showed that mutating Asn406 to Ala or Cys in $Na_V1.5$

conferred "T-type–like" blocking action of mibefradil, a putative blocker of T-type Ca^{2+} channels, on Na^+ channels and yielded slower inactivation. An alignment of the P-loop region of the four repeats of $Ca_V3.1$, $Ca_v3.2$, and $Ca_v3.3$ thought to generate T-type Ca^{2+} currents (Perez-Reyes, 2003; Vassort et al., 2006) shows significant homology with that of various mammalian Na^+ genes (Fig. 1). Tetrodotoxin (TTX) and saxitoxin (STX) are two structurally related heterocyclic guanidinium marine toxins that potently inhibit voltage-gated Na^+ channels by an interaction with several residues in the P-loop as indicated in Fig. 1 (labeled in red). In view of the structural similarities within or near the pore region of the two classes of channels and the possibility that they may have evolved from a common ancestor, we wondered whether these toxins also interact with T-type Ca^{2+} channels. We examined the effects of TTX and STX from several commercial sources on I_{CaT} recorded from canine atrial myocytes or from HEK 293 cells transfected with $Ca_V3.1$, $Ca_V3.2$, or $Ca_V3.3$. TTX exerted no significant effect on the magnitude of native I_{CaT} and I_{CaT} generated by either $Ca_V3.1$ or $Ca_V3.2$, the two isoforms predominantly expressed in heart (Vassort et al., 2006), while it inhibited $Ca_V3.3$-induced I_{CaT}. Interestingly, for both native I_{CaT} and $Ca_V3.1$- or $Ca_V3.2$-induced I_{CaT}, TTX partially relieved the blockade of this current by Ni^{2+}. Finally, STX directly inhibited I_{CaT} in dog atrial cells and that elicited by expression of all three Ca_V3 subclasses. Our studies further extend the notion that voltage-gated Na^{2+} and Ca^{2+} channels share signature properties and may have arisen from a common ancestor.

MATERIALS AND METHODS

This investigation conforms to the Guide for the Care and Use of Laboratory Animals published by the NIH and the guidelines of the Canadian Council on Animal Care, and was approved by the Montreal Heart Institute Animal Care Committee.

Cell Dispersion Technique

Adult mongrel dogs (20–30 kg) were anesthetized with morphine (2 mg/kg s.c.) and α-chloralose (120 mg/kg i.v.) and mechanically ventilated. The heart was removed after intra-atrial injection of heparin (10,000 U), immersed in 2 mM Ca^{2+}-containing Tyrode solution, and the left atrium perfused via the circumflex artery with Tyrode solution until free of blood. The perfusate was then switched to nominally Ca^{2+}-free Tyrode solution for 20 min, after which 110 U/ml collagenase (Type II, Worthington) and 0.1% BSA were added. Perfusion solutions were saturated with 100% O_2 at 37°C. Cells were dispersed by gentle trituration in Tyrode's containing 10 μM Ca^{2+}. The cells were kept at room temperature in Tyrode solution containing 100 μM Ca^{2+} and 0.1% BSA for use within 8 h. The composition of the Tyrode solution was as follows (mM): NaCl 136, KCl 5.4, $MgCl_2$ 1.0, $CaCl_2$ 2, NaH_2PO_4 0.33, glucose 10, and HEPES 10, pH adjusted to 7.4 with NaOH.

Cell Culture and Transient Transfection

tsA-201 cells were grown and transiently transfected with expression plasmids for hCav3.1, hCav3.2, or $hCa_V3.3$ constructs and πH3-CD8, containing the cDNA of the T cell antigen CD8 to identify effectively transfected cells. In brief, cells were grown to 85% confluence at 37°C (5% CO_2) in Dulbecco's modified Eagle's medium (DMEM) (+10% FBS, 200 U/ml penicillin, and 0.2 mg/ml streptomycin, Invitrogen) in 35-mm cell culture plastic Petri dishes and transfected with hCav3.1, hCav3.2, or hCav3.3 channel α_1 subunits (8 μg) and CD8 marker (1 μg) by the calcium phosphate method for 8 h. After transfection, cells were dissociated with trypsin (0.25%)-EDTA and plated on glass coverslips. Experiments were performed 24–48 h after transfection.

Electrophysiology and Data Analysis

Macroscopic currents were recorded from Ca^{2+}-tolerant canine atrial myocytes using the whole-cell patch clamp technique (35.5 ± 0.5°C). With tips ~1 μm in diameter, patch pipette resistance ranged between 2 and 4 MΩ when the micropipette was filled with the internal solution containing (in mM) CsCl 120, TEA 20, $MgCl_2$ 1, MgATP 5, HEPES 10, GTP.Na 0.1, and EGTA 10, pH adjusted to 7.2 with CsOH. Voltage clamp protocols were computer driven using Digidata 1200 series acquisition system with PClamp software (v. 8.0 or 9.2) and an Axopatch 200A amplifier (Molecular Devices). Pipette and stray capacitance, as well as series resistance were compensated for in all experiments. Membrane currents were low-pass filtered at 1 or 2 kHz (4-pole Bessel filter) before being acquired at a sampling rate of 2 or 5 kHz. After gaining whole-cell access, myocytes were held at the standard holding potential −90 mV, and cell dialysis was allowed to proceed for at least 5 min before any voltage clamp protocol was initiated. To minimize the undesirable effects of I_{CaL} rundown on the measurement of low threshold I_{Ca}, we used a voltage clamp protocol consisting of two test pulses (TP1 and TP2) to different voltages separated by a 500-ms interval at −50 mV. The current elicited by TP1 comprised both low and high threshold Ca^{2+} currents, and that evoked by TP2 mainly consisted of I_{CaL}. Digital subtraction of I_{CaL} from total Ca^{2+} current recorded during TP1 yielded the low threshold T-type I_{Ca} (I_{CaT}). The bath solution for Ca^{2+} current recordings contained (in mM) TEA 136, CsCl 5.4, $MgCl_2$ 1, $CaCl_2$ 1.8, HEPES 10, glucose 5.5, and 4-aminopyridine (4-AP) 2, pH adjusted to 7.35 with CsOH. In all cells studied, cell membrane capacitance was estimated by integrating (with Clampfit 8.0 or 9.2, Molecular Devices) the mean of five consecutive capacitative current transients elicited by 20-ms test pulses from −50 to −60 mV.

All experiments on HEK-293 cells transfected with $hCa_V3.1$, $hCa_V3.2$, or hCav3.3 were performed at room temperature with a bathing solution containing 2 mM Ca^{2+} (in mM): 128 CsCl, 2 $CaCl_2$, 1.5 $MgCl_2$, 10 HEPES, and 25 D-glucose; pH 7.4 (adjusted with CsOH). In the experiments designed to examine the effects of EDTA on the response of I_{CaT} to Na^+ channel toxins (see Fig. S2, available at http://www.jgp.org/cgi/content/full/jgp.200709883/DC1), all solutions containing Ni^{2+} were adjusted to take into account the buffering effect of EDTA on this cation and ensure that the solutions with and without EDTA had equivalent free Ni^{2+} concentrations. In the presence of 100 μM EDTA, the total added Ni^{2+} concentrations to achieve either 15, 550, or 750 μM free $[Ni^{2+}]_o$ to block respectively $Ca_V3.1$, $Ca_V3.2$, or $Ca_V3.3$ were calculated using WinMAXC (v. 2.5, Chris Patton, http://www.stanford.edu/~cpatton/downloads) and were as follows (in mM): 15 μM free $[Ni^{2+}]_o$: 115 μM total $[Ni^{2+}]_o$; 550 μM free $[Ni^{2+}]_o$: 650 μM total $[Ni^{2+}]_o$; 750 μM free $[Ni^{2+}]_o$: 850 μM total $[Ni^{2+}]_o$. Whole-cell patch clamp recordings were performed on cells positive for CD8 antibody coated beads, using an Axopatch 200B (Molecular Devices) amplifier and Clampex 9.2 software (Molecular Devices), low-pass filtered at 1 kHz and digitized at 10 kHz. Borosilicate glass pipettes (2.5–4 MΩ) were filled with internal solution (in mM): 135 CsCl, 10 EGTA, 2 $CaCl_2$, 10 HEPES, and 1 $MgCl_2$; pH 7.2 (adjusted with CsOH). Series resistance was compensated to 80% of the initial value. Steps of 250 ms duration to −40 mV (5 s interval)

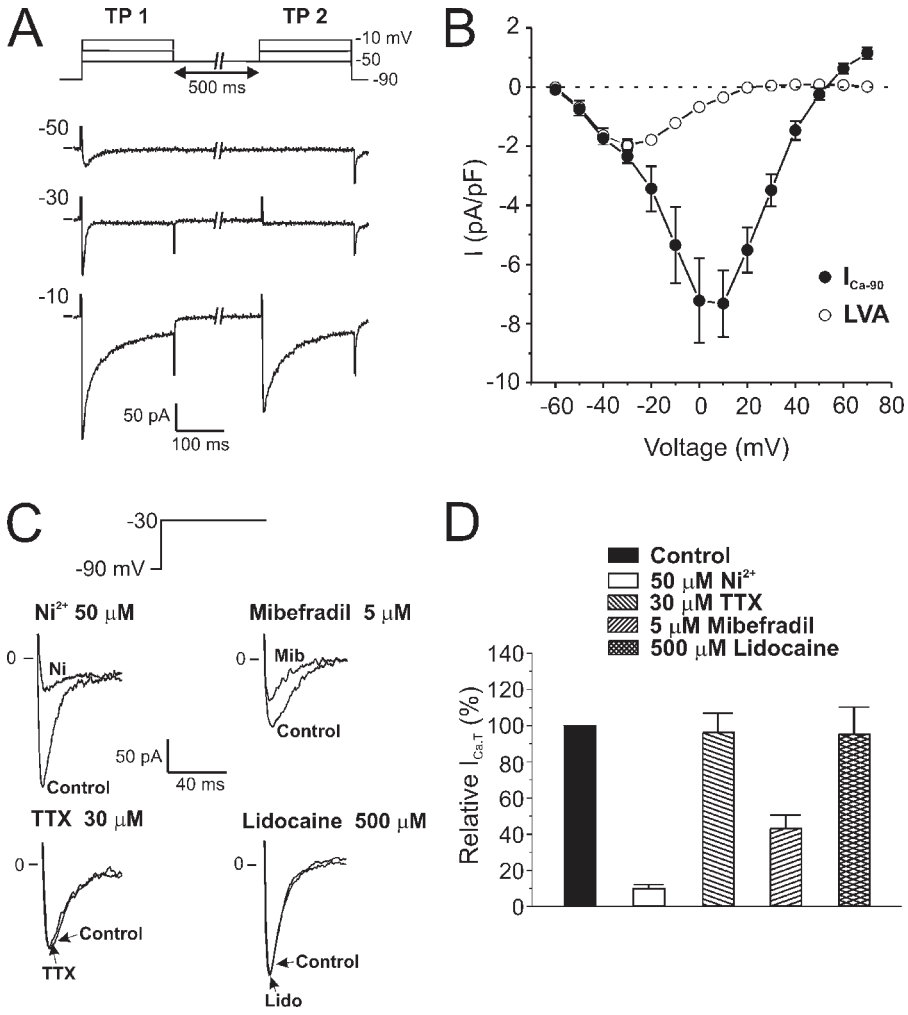

Figure 2. Biophysical and pharmacological properties of low and high voltage–activated Ca^{2+} currents in dog atrium. (A) Representative current traces recorded during steps to indicated voltages by the voltage clamp protocol shown at the top. (B) Mean *I-V* curves of total I_{Ca} ($I_{Ca\text{-}90}$) elicited by the first test pulse (TP1), and the low voltage-activated I_{Ca} (LVA) obtained by subtracting the currents elicited by TP2 from those evoked by TP1 ($n = 6$). LVA peaks at −30 mV and reverses between +30 and +60 mV, consistent with I_{CaT} previously described in cardiac cells. (C) Four sets of superimposed typical current traces recorded from different cells are shown. Currents were elicited by steps to −30 mV (or to −40 mV for the right top set of traces) from HP = −90 mV before and after application of different compounds as indicated. Short bars to left of current traces indicate zero current level. Low threshold inward current was inhibited by nickel (Ni^{2+}) and mibefradil (Mib), two putative T-type Ca^{2+} channel blockers, but was insensitive to the Na^+ channel antagonist tetrodotoxin (TTX) and lidocaine (Lido). (D) Bar graph summarizing the effects of the various compounds for experiments similar to those illustrated in C. As in C, each compound was tested in different cells. Peak inward current is expressed as mean ± SEM % relative to the control value (filled bar). LVA was inhibited 90% by 50 μM Ni^{2+} (Control: −99 ± 6 pA, Ni^{2+}: −10 ± 2 pA, $n = 16$) and 57% by 5 μM mibefradil (Control: −132 ± 19 pA, mibefradil: −57 ± 10 pA, $n = 6$), but was not significantly affected by 30 μM TTX (Control: −73 ± 7 pA, TTX: −70 ± 8 pA, $n = 5$) or 500 μM lidocaine (Control: −116 ± 21 pA, lidocaine: −111 ± 17 pA, $n = 3$). The source of TTX for all these experiments was Calbiochem.

were given to the cells from a holding potential of −90 mV to monitor the magnitude of the current.

Reagents

All reagents were purchased from Sigma-Aldrich or Merck KGaA. Tetrodotoxin (TTX) was purchased from Calbiochem (dog atrial cell experiments) or Alomone Laboratories (dog atrial and transfected HEK cell experiments), whereas saxitoxin (STX) was obtained from Calbiochem (dog atrial cell experiments), Sigma-Aldrich (dog atrial cell experiments), or from the Institute for Marine Biosciences, NRC-IMB (Halifax, Nova Scotia, Canada; transfected HEK cell experiments).

Statistical Analysis

Membrane currents were analyzed with Clampfit 8.0 and/or 9.2 (Molecular Devices). Offline leak subtraction was performed in Clampfit by digital subtraction using scaled currents that did not elicit time-dependent currents. The software Origin 7.5 (OriginLab Corp.) was used to calculate the best fit to the dose-dependent response of I_{CaT} to Ni^{2+}, TTX, and STX using weighed least-squares fitting routines to a Logistic function.

All pooled data are expressed as means ± SEM. Both unpaired and paired Students *t* tests were used to determine the statistical difference between two means (Statistica for Windows 99, version 5.5). Comparisons among multiple means were performed using one-way ANOVA with a Newman-Keuls (Statistica for Windows, Statsoft) or Bonferroni post-hoc tests (OriginLab Corp.). Comparisons of I_{CaT} amplitudes obtained in control, Ni^{2+}-treated, and Ni^{2+} plus TTX-treated groups over voltage range from −40 to −10 mV were performed using two-way ANOVA (Origin 7.5). A P value of <0.05 was considered to indicate statistical significance.

Online Supplemental Material

The online supplemental material (available at http://www.jgp.org/cgi/content/full/jgp.200709883/DC1) includes data showing the effects of low concentrations of external Na^+ (0.05 to 4 mM) and TTX (30 μM) on the low threshold inward Ca^{2+} current recorded from dog atrial myocytes, and the impact of buffering heavy metals with EDTA (100 μM) on the responses of expressed $Ca_V3.1$–$Ca_V3.3$ to STX and TTX. The data presented in Fig. S1 provides additional evidence that the low threshold Ca^{2+} current in atrial myocytes consists of a T-type Ca^{2+} current only and is not the result of a TTX-sensitive Ca^{2+} current ($I_{Ca(TTX)}$) as identified in cardiac myocytes of some species in the absence of external Na^+. Fig. S2 reports the lack of effect of EDTA on the responses to STX and TTX of T-type Ca^{2+} current evoked by the expression of either

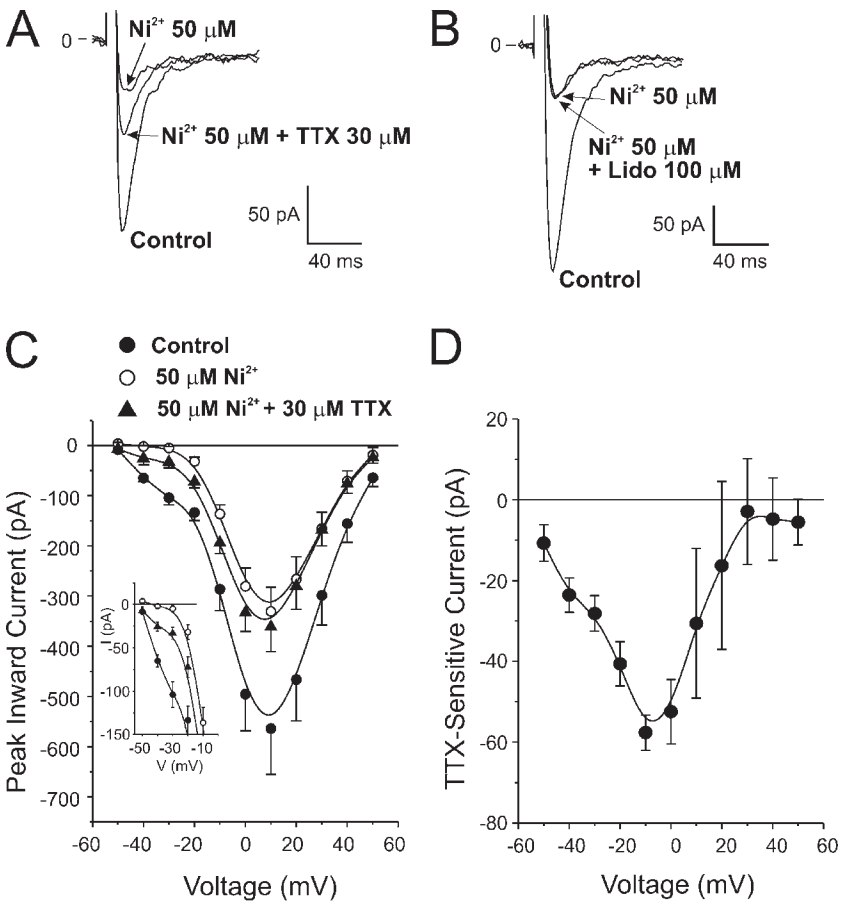

Figure 3. TTX, but not lidocaine relieves the blockade of I_{CaT} by Ni^{2+} in dog atrium. (A) Current traces elicited by voltage steps from −90 to −30 mV were recorded in the absence and presence of 50 μM Ni^{2+}, and after the further addition of 30 μM TTX. Notice that TTX partially alleviated the block mediated by nickel. (B) Sample current traces elicited by voltage steps from −90 to −30 mV recorded in the absence and presence of 50 μM Ni^{2+}, and after the further addition of 100 μM lidocaine (Lido). (C) Mean *I-V* relationships for peak inward current evoked by steps ranging from −50 to +50 mV from HP = −90 mV in control conditions (filled circles), after the addition of 50 μM Ni^{2+} (empty circles) and in the combined presence of Ni^{2+} and TTX (filled triangles; $n = 7$). Inset shows an expanded portion of the *I−V* to better illustrate the effects of TTX. (D) Voltage dependence of TTX-sensitive current derived from C by digital subtraction of current recorded in the presence of Ni^{2+} from that recorded in the presence of both Ni^{2+} and TTX. The source of TTX for all these experiments was Calbiochem.

one of the three Ca_V3 subunits in HEK-293 cells, which indicates that the effects of the toxins on I_{CaT} are not due to the presence of heavy metal contaminants in the commercial toxin samples.

RESULTS

Identification of I_{CaT} in Canine Atrial Cells

We first examined whether low and high threshold inward Ca^{2+} currents could be unequivocally identified in canine atrial cells superfused with a Na^+-free medium containing physiological Ca^{2+} concentration (1.8 mM). Fig. 2 A shows three sample membrane currents recorded in the same cell using the protocol shown at the top of this panel. A fast transient inward current was apparent at −50 and −30 mV during an initial 200-ms test pulse (TP1) from HP = −90 mV, and was completely inactivated during the second test pulse (TP2) to −30 mV (now elicited from a preconditioning potential of −50 mV). The inward current elicited by TP1 to −10 mV was clearly larger, and activated and inactivated more quickly than that evoked during TP2. Fig. 2 B shows the mean current–voltage (*I–V*) relationships ($n = 6$) for peak inward current recorded during TP1 ranging from −60 to +70 mV (filled circles), and low voltage–activated Ca^{2+} current (LVA) obtained from digital subtraction of the currents evoked by TP2 from those elicited by TP1 (empty circles). Examination of the *I-V* curve of the LVA shows that this current activated between −60 and −50 mV, peaked near −30 mV, and reversed between +30 and +60 mV. In contrast, the high threshold inward current activated between −40 and −30 mV, reached a maximum between 0 and +10 mV, and reversed near +50 mV.

The pharmacological data presented in Fig. 2 (C and D) support the contention that LVA is mainly composed of I_{CaT} and is not due to a Ca^{2+} entry pathway that is sensitive to block by TTX (so-called $I_{Ca(TTX)}$; Lemaire et al., 1995; Aggarwal et al., 1997; Cole et al., 1997; Santana et al., 1998; Sha et al., 2003). LVA was selectively inhibited by the T-type Ca^{2+} channel blockers Ni^{2+} (50 μM; $P < 0.05$) and mibefradil (5 μM; $P < 0.05$), but was unaltered by 30 μM TTX ($P > 0.05$) or 500 μM of the local anesthetic lidocaine ($P > 0.05$), both of which block Na^+ current (I_{Na}). Another set of experiments also shows that LVA elicited at negative potentials is unaffected by 50 μM Na^+ in the external medium ($P > 0.05$), a concentration previously shown to partially inhibit $I_{Ca(TTX)}$ (Cole et al., 1997; Alvarez et al., 2004), while higher concentrations of Na^+ led to the appearance of a faster TTX-sensitive inward current consistent with cardiac I_{Na} (Fig. S1, available at http://www.jgp.org/cgi/content/full/jgp.200709883/DC1). These results are consistent

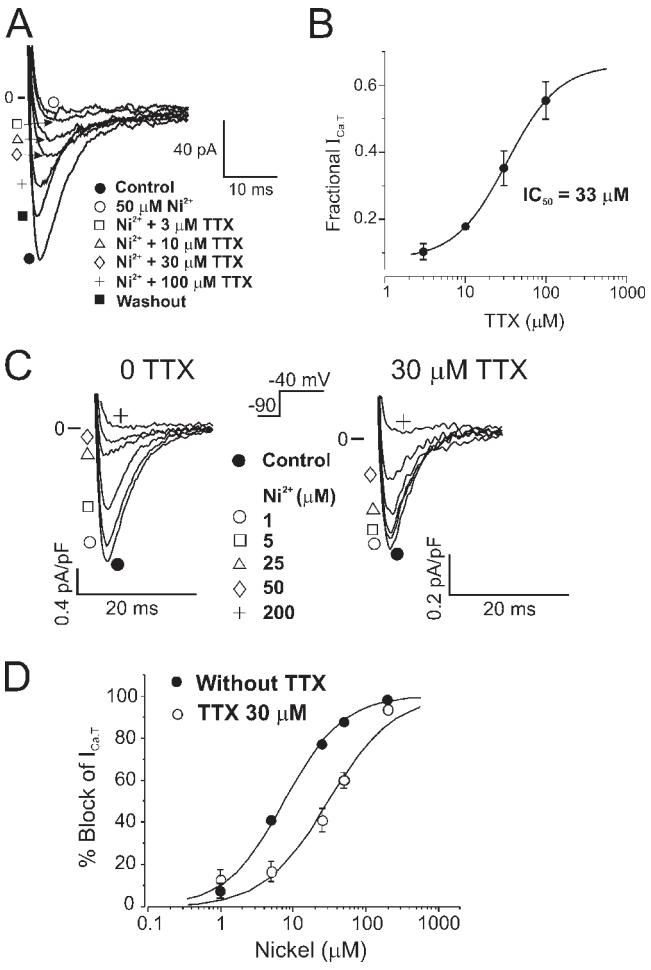

Figure 4. Concentration dependence of TTX relief of I_{CaT} block by Ni^{2+} in dog atrial myocytes. (A) Typical current traces elicited by voltage steps from −90 to −40 mV under control conditions (Control, filled circle), in the presence of 50 μM Ni^{2+} alone (empty circle), with different concentrations of TTX in the continued presence of Ni^{2+} (empty square, triangle, and diamond, and cross) and after washout of all drugs (filled square). (B) Dose–response curve of TTX relief of block of I_{CaT} by Ni^{2+} obtained from two cells. The curve represents a sigmoidal fit to the data points, yielding an IC_{50} of 33 μM for the TTX relief of Ni^{2+} block on the channel. Each data point is a mean ± SEM of fractional I_{CaT} ([Ni^{2+} + TTX]/[Control]). (C) Representative current traces elicited by voltage steps from −90 to −40 mV in two different cells exposed to various concentrations of Ni^{2+}, in the absence (left) or presence (right) of 30 μM TTX. (D) Dose–response curves for Ni^{2+} block of I_{CaT}, with or without TTX. n = 5 cells/group. The source of TTX for all these experiments was Calbiochem.

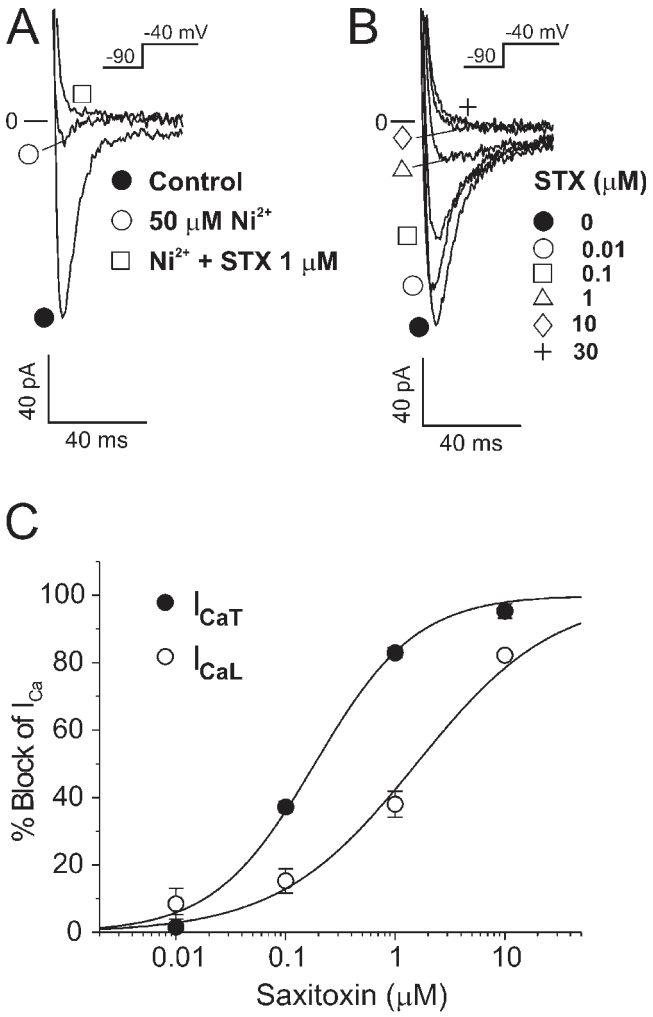

Figure 5. Effects of STX on I_{CaT} and I_{CaL} in dog atrial myocytes. (A) Current traces recorded during steps from −90 to −40 mV (inset) in a typical cell in the absence (Control, filled circle) or presence of 50 μM Ni^{2+} (empty circle), and after the further addition of 1 μM saxitoxin (STX, empty square). 1 μM STX abolished the residual current left in the presence of 50 μM Ni^{2+}. Similar results were obtained in three cells. (B) Current traces elicited by voltage steps from −90 to −40 mV (inset) in a typical cell exposed to increasing concentrations of STX (empty symbols and cross). As evident, 10 μM STX was sufficient to abolish I_{CaT}. (C) Dose–response curves for STX inhibition of I_{CaT} and I_{CaL}, with estimated EC_{50}s of 185 nM for I_{CaT} (filled circles) and 1.6 μM for I_{CaL} (empty circles). The effects of STX on I_{CaT} and I_{CaL} were evaluated in the same cell using a triple-pulse protocol that was composed of the double-pulse protocol (see Materials and methods) for I_{CaT} recording and a third step from −50 to + 10 mV separated by a 500-ms interval to elicit I_{CaL} (n = 6). The source of STX for all these experiments was Calbiochem.

with the existence of two types of inward Ca^{2+} current in this cardiac preparation with distinct kinetics and voltage dependence resembling those previously reported in other systems: low threshold T-type (I_{CaT}) and high threshold L-type (I_{CaL}) Ca^{2+} currents (Bean, 1985; Mitra and Morad, 1986; McDonald et al., 1994; Fareh et al., 2001).

Relief of Ni^{2+}-induced Blockade of Native I_{CaT} by TTX

While examining the pharmacological profile of the LVA in our preparation, we found that TTX does in fact interact with I_{CaT} but in a very peculiar manner. Fig. 3 A shows a sample experiment demonstrating this effect. In control conditions, a 200-ms step to −30 mV from HP = −90 mV evoked a typical I_{CaT}, which was inhibited >80% by 50 μM Ni^{2+}. In the continued presence of Ni^{2+}, application of 30 μM TTX partially relieved the block exerted by Ni^{2+} ($P < 0.001$). This sustained effect was consistently

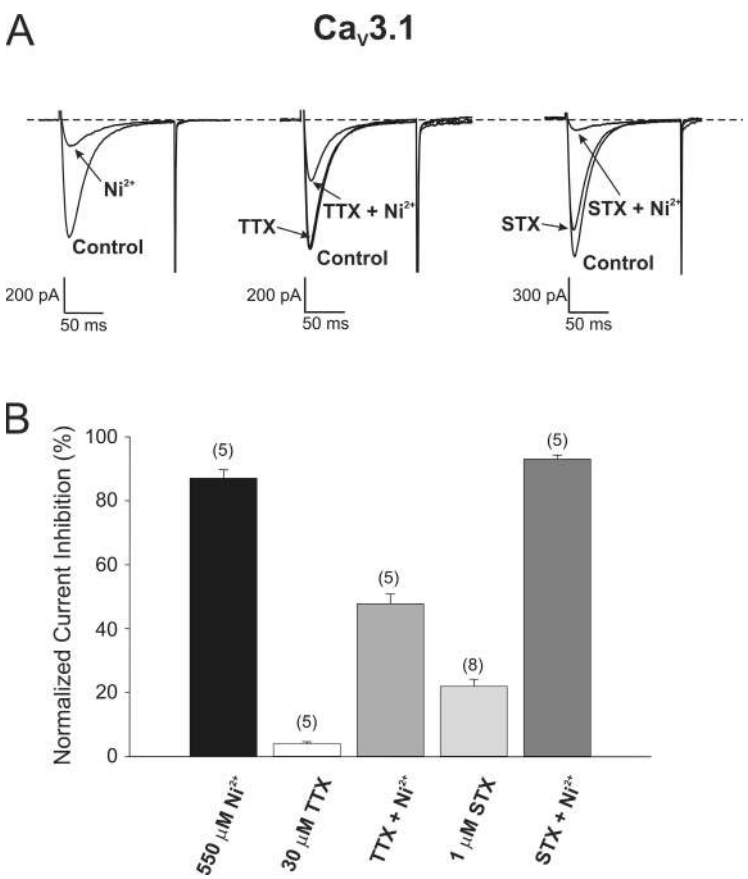

Figure 6. Effects of TTX and STX on $Ca_V3.1$ expressed in HEK-293 cells. (A) Typical T-type Ca^{2+} current recordings showing the effects of 550 μM Ni^{2+} alone (left), the effects of 30 μM TTX in the presence of 550 μM Ni^{2+} (middle), and the effects of 1 μM STX in the absence or presence of 550 μM Ni^{2+} (right). Please note that the leftward and middle traces were obtained from the same cell while the ones on the righthand side were from a different experiment. As for the native T-type Ca^{2+} current, TTX attenuated the block of $Ca_V3.1$-induced current by Ni^{2+} and STX produced a significant inhibition of this current. (B) Bar graph showing pooled data from similar experiments to those shown in A. The data were expressed as mean ± SEM % block of peak inward current. The numbers in parentheses reflect the number of experiments. TTX and STX for all these experiments were respectively purchased from Alomone Laboratories and the Institute for Marine Biosciences, NRC-IMB.

observed in all 16 myocytes studied and took place regardless of the order of application of Ni^{2+} or TTX. Fig. 3 B illustrates that the effect of TTX on Ni^{2+}-induced block of I_{CaT} was not shared by the structurally unrelated Na^+ channel antagonist lidocaine. Moreover, the inhibition of I_{CaT} by an 8–10-min exposure to 5 μM mibefradil could not be reversed by 30 μM TTX; the amplitude of I_{CaT} elicited at −30 mV from HP = −90 mV was −67 ± 14 pA in the presence of 5 μM mibrefradil, and −61 ± 13 pA after exposure to mibefradil and TTX (n = 3; $P > 0.05$). Fig. 3 C shows mean *I-V* relationships for peak inward current recorded from HP = −90 mV in control conditions, after the addition of Ni^{2+}, and in the combined presence of Ni^{2+} and 30 μM TTX. Nickel abolished I_{CaT} and partially suppressed I_{CaL}; for example, the inward current recorded at +20 mV, which mainly consists of I_{CaL} (see Fig. 2 B), was inhibited 46% by Ni^{2+}, a result consistent with previous studies in cardiac myocytes (McDonald et al., 1994; Hobai et al., 2000). Most importantly, this plot shows that the partial relief of Ni^{2+} block by TTX was mainly apparent between −40 and ∼+10 mV, which supports the idea that TTX interacts with I_{CaT} but not I_{CaL}. Two-way ANOVA analysis revealed a significant difference ($P < 0.05$) of I_{CaT} densities obtained in control, Ni^{2+}-treated, and Ni^{2+} plus TTX-treated conditions over the voltage range from −40 to −10 mV. It also suggests that the relief of the Ni^{2+} block of I_{CaT} by TTX is voltage dependent, being attenuated by membrane depolarization. This observation would be consistent with an electrostatic repulsion of the TTX molecule as it carries a net positive charge at physiological pH.

TTX dose dependently relieved the block of I_{CaT} induced by 50 μM Ni^{2+} (Fig. 4 A). Data pooled from several experiments showed that TTX relieved the block produced by Ni^{2+} with an IC_{50} of 33 μM (Fig. 4 B). We next explored the concentration dependence of the block exerted by Ni^{2+} in the presence and absence of TTX. Fig. 4 C shows representative current recordings obtained in two different cells. Both cells were exposed in sequence to increasing concentrations of Ni^{2+} ranging from 1 to 200 μM, with (righthand side) or without 30 μM TTX (lefthand side) throughout. These experiments clearly show that Ni^{2+} was more effective at inhibiting I_{CaT} in the absence than in the presence of TTX. Fig. 4 D shows mean data from such similar experiments. The Na^+ channel toxin induced a rightward shift of the dose–response curve without affecting the slope of the relationship; the IC_{50} was 7.6 and 30 μM in the absence and presence of TTX, respectively. These results support the notion that TTX interferes with Ni^{2+} block of the I_{CaT} channel through a competitive interaction.

The commercial source of the TTX used in the experiments shown in Figs. 3 and 4 was Calbiochem. We also examined the effects of TTX from a different source

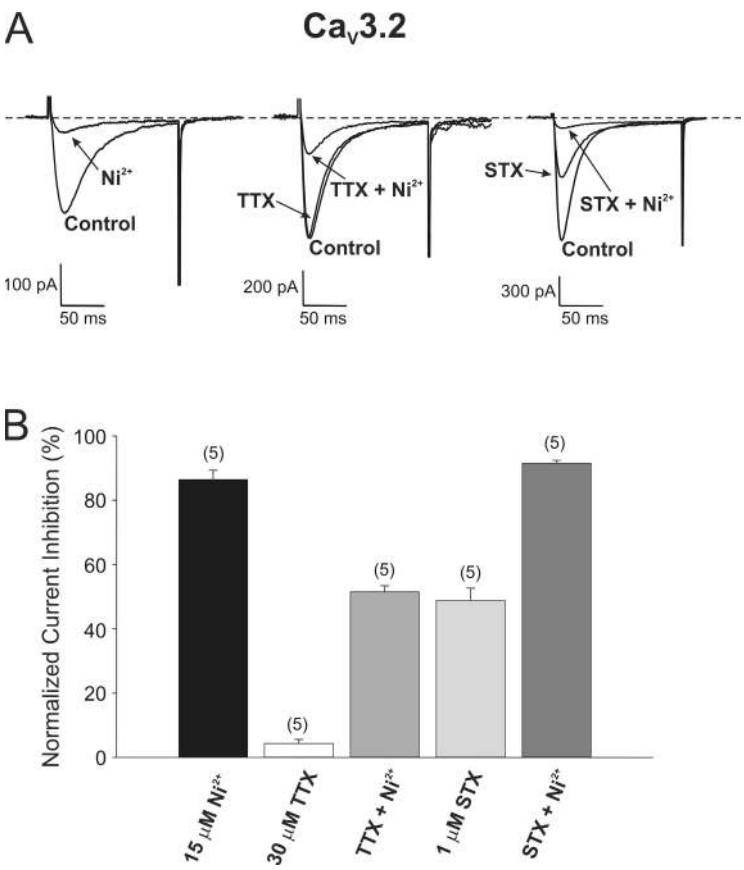

Figure 7. Effects of TTX and STX on $Ca_V3.2$ expressed in HEK-293 cells. (A) Typical T-type Ca^{2+} current recordings showing the effects of 15 μM Ni^{2+} alone (left), the effects of 30 μM TTX in the presence of 15 μM Ni^{2+} (middle), and the effects of 1 μM STX in the absence or presence of 15 μM Ni^{2+} (right). Please note that the leftward and middle traces were obtained from the same cell while the ones on the right hand side were from a different experiment. As for the native T-type Ca^{2+} current, TTX attenuated the block of $Ca_V3.1$-induced current by Ni^{2+} and STX produced a significant inhibition of this current. (B) Bar graph showing pooled data from similar experiments to those shown in A. The data were expressed as mean ± SEM % block of peak inward current. The numbers in parentheses reflect the number of experiments. TTX and STX for all these experiments were respectively purchased from Alomone Laboratories and the Institute for Marine Biosciences, NRC-IMB.

and found quantitatively similar results. TTX (30 μM) purchased from Alomone Laboratories had no significant on I_{CaT} evoked at −30 mV from HP = −90 mV (Control: 120 ± 32 pA; TTX: 103 ± 23 pA, n = 4, P > 0.05). As for TTX from Calbiochem, it significantly reduced the block by 50 μM Ni^{2+} (Ni^{2+}: 82.9 ± 1.5% block; Ni^{2+} + TTX: 44.5 ± 4.9% block, n = 4, P < 0.01).

Saxitoxin Inhibits both Native I_{CaT} and I_{CaL}

We next tested the hypothesis that another marine toxin, saxitoxin (STX), which like TTX blocks Na^+ channels (Hille, 2001), might also influence I_{CaT} in canine atrial myocytes. As illustrated in Fig. 5 and in contrast to TTX, STX (Calbiochem) potently inhibited I_{CaT} in the presence of 50 μM Ni^{2+} (Fig. 5 A; P < 0.05), and dose dependently reduced this current in the absence of this divalent cation (Fig. 5 B). Fig. 5 C shows the dose–response curves for the inhibition of I_{CaT} and I_{CaL} by STX. In these experiments, the effects of STX on the two inward currents were evaluated in the same cell using a triple-pulse protocol. The magnitude of T-type Ca^{2+} current was first estimated by the double-pulse protocol described in the Materials and methods. Saxitoxin inhibited I_{CaT} with an IC_{50} = 185 nM. The toxin also suppressed I_{CaL} in a concentration-dependent manner with an IC_{50} = 1.6 μM, which is a slightly less potent inhibition than that reported by Su et al. (2004) for STX block of I_{CaL} in mouse ventricular myocytes (K_d ∼0.3 μM). In contrast to the complete STX block observed in our study, they found that maximum block was partial (∼50%). STX (1 μM) from Sigma-Aldrich blocked I_{CaT} by 51.5 ± 4.2% (n = 7; P < 0.01), somewhat less potently than that from Calbiochem (Fig. 5 C; ∼83% block) but similar to that produced by STX from the Institute for Marine Biosciences on $Ca_V3.2$ (∼51% block; see Fig. 7).

Effects of TTX and STX on Transiently Expressed I_{CaT}

It is now well established that cardiac I_{CaT} results mainly from the expression of $Ca_V3.1$ and/or $Ca_V3.2$ (Perez-Reyes, 2003; Vassort et al., 2006), although one study reported the expression of mRNA transcripts for $Ca_V3.1$, $Ca_V3.2$, and $Ca_V3.3$ in dog atrium, ventricle, and Purkinje fibers (Han et al., 2002). Fig. 6 A shows sample recordings of I_{CaT} from h$Ca_V3.1$-transfected cells elicited by repetitive 250-ms steps to −40 mV from a holding potential of −90 mV. Application of Ni^{2+} (550 μM) inhibited $Ca_V3.1$ current ∼75%. Such a high Ni^{2+} concentration was necessary to achieve substantial block of the current in accordance with the reported sensitivity of $Ca_V3.1$ to this blocker (IC_{50} ≈ 250 μM; Perez-Reyes, 2003). Similar to cardiac I_{CaT} (Fig. 2 C and Fig. 3), 30 μM TTX had no direct effect on the current (middle set of traces). However, the same concentration of Ni^{2+} was clearly less effective at blocking $Ca_V3.1$ in the presence of TTX (middle recordings). Again, similar to native I_{CaT} (Fig. 5), 1 μM STX directly inhibited $Ca_V3.1$ and

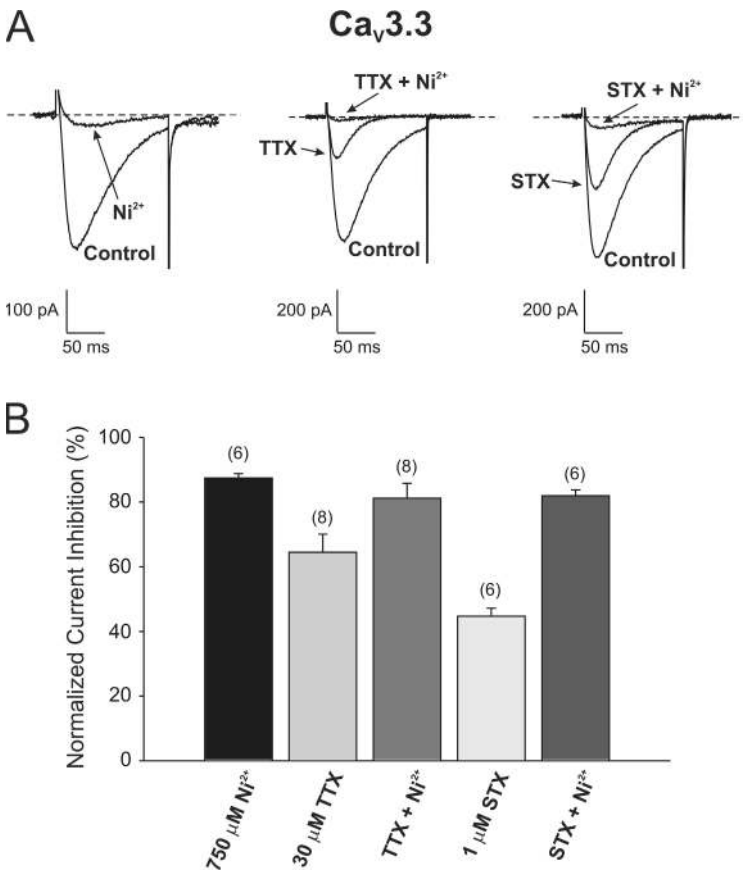

Figure 8. Effects of TTX and STX on $Ca_V3.3$ expressed in HEK-293 cells. (A) Typical T-type Ca^{2+} current recordings obtained from HEK-293 cells transiently transfected with $Ca_V3.3$. This panel illustrates the effects of 750 µM Ni^{2+} alone (left), those of 30 µM TTX in the absence or presence of 750 µM Ni^{2+} (middle), and the effects of 1 µM STX in the absence or presence of 750 µM Ni^{2+} (right). As for Figs. 6 and 7, current traces were elicited by voltage steps to −40 mV from a holding potential of −90 mV. The three families of traces are from different cells. (B) Bar graph summarizing the effects of different blockers for experiments similar to those illustrated in A. The data were expressed as mean ± SEM % block of peak inward current. The numbers in parentheses reflect the number of experiments. TTX and STX for all these experiments were respectively purchased from Alomone Laboratories and the Institute for Marine Biosciences, NRC-IMB.

addition of Ni^{2+} led to further inhibition of the current. Fig. 6 B provides a summary of mean data from five to eight experiments with TTX and STX, respectively. A similar analysis was performed on $Ca_V3.2$ and the results are displayed in Fig. 7 following an identical format to the results presented in Fig. 6. A reduced concentration of Ni^{2+} (15 µM) was used to probe $Ca_v3.2$ channels because of the higher affinity of Ni^{2+} for $Ca_V3.2$ (IC_{50} ≈ 12 µM; Perez-Reyes, 2003). A similar trend was observed for this Ca^{2+} channel isoform, including lack of effect of TTX, attenuation of Ni^{2+} blockade by TTX, direct inhibition by STX, and maximal block by the combined addition of Ni^{2+} and STX, which was not significantly different from the level of block achieved by Ni^{2+} alone (Fig. 7 B). In contrast to the lack of effect of TTX on $Ca_v3.1$ and $Ca_v3.2$, the toxin at a concentration of 30 µM inhibited I_{CaT} mediated by $Ca_v3.3$ by >60% (Fig. 8 A, middle set of traces). The addition of 750 µM Ni^{2+} in the presence of TTX led to further block of I_{CaT}, which was similar to that produced by Ni^{2+} alone (Fig. 8 A, leftward set of traces). The higher concentration of Ni^{2+} was chosen to produce similar block of I_{CaT} and is consistent, as for I_{CaT} arising from the expression of $Ca_V3.1$, with the low affinity of $Ca_V3.3$-mediated I_{CaT} for Ni^{2+} (IC_{50} ≈ 216 µM; Perez-Reyes, 2003). Finally, 1 µM STX produced similar inhibitory effects on $Ca_V3.3$-elicited I_{CaT} to those observed on currents arising from expressed $Ca_V3.1$ (Fig. 6) or $Ca_V3.2$ (Fig. 7), with a similar response to Ni^{2+} in the presence of the toxin (Fig. 8 A, rightward set of traces). Fig. 8 B summarizes the data pooled from six to eight cells. All observed effects of the toxins, with or without Ni^{2+}, on Ca_V3-induced I_{CaT} were unaffected by the addition in the superfusate of 100 µM EDTA to chelate heavy metals that might contaminate the toxin samples (Fig. S2). These results are in agreement with the paradigm that the well-characterized Na^+ channel toxins TTX and STX interact with the α-subunit of native and cloned T-type Ca^{2+} channels.

DISCUSSION

In the present study, we provide evidence that the Na^+ channel antagonists tetrodotoxin and saxitoxin both interact with native and cloned T-type Ca^{2+} channels. Our data indicate that while TTX produced no effect on cardiac I_{CaT}, and $Ca_V3.1$ and $Ca_V3.2$, the toxin significantly attenuated the block produced by Ni^{2+}. In contrast, STX exerted relatively high affinity block of cardiac I_{CaT} and $Ca_V3.1$–3.3, and did not affect Ni^{2+}-induced inhibition of I_{CaT}; TTX produced similar effects on $Ca_V3.3$. These results point to common toxin-binding sites on I_{CaT} and I_{Na} channels and support the hypothesis that voltage-dependent T-type Ca^{2+} and Na^+ channels may have evolved from a common ancestor.

Low Threshold Inward Current in Dog Atrial Myocytes is a T-type Ca^{2+} Current

In the absence of external sodium ions, low voltage–activated inward calcium current (LVA) was consistently recorded in all canine atrial myocytes studied. With physiological Ca^{2+} in the bathing medium, this current shared many properties with T-type Ca^{2+} current measured in cardiac muscle cells (Bean, 1985; Mitra and Morad, 1986; McDonald et al., 1994; Zhang et al., 2000; Fareh et al., 2001) and α_{1G} and α_{1H} subunits expressed in mammalian cell lines (Cribbs et al., 1998; Monteil et al., 2000; Satin and Cribbs, 2000; Cribbs et al., 2001); the current (1) activated at potentials more negative than −40 mV and was completely inactivated at a holding potential of −50 mV, (2) displayed faster kinetics of activation and inactivation than L-type Ca^{2+} current, and (3) was blocked by mibefradil or Ni^{2+}. LVA was likely not the product of a TTX-sensitive Ca^{2+} entry mechanism since the latter pathway has been shown to be inhibited by TTX (Lemaire et al., 1995; Cole et al., 1997; Alvarez et al., 2004) or low concentrations (10–200 μM) of external Na^+ (Cole et al., 1997; Alvarez et al., 2004), but is unaffected by Ni^{2+} concentrations up to 250 μM (Lemaire et al., 1995; Aggarwal et al., 1997; Cole et al., 1997; Heubach et al., 2000; Alvarez et al., 2004). We therefore conclude that LVA in canine atrial cells is generated by a T-type Ca^{2+} channel that is most likely primarily encoded by $Ca_V3.2$ since the IC_{50} for the block of I_{CaT} by Ni^{2+} (7.6 μM) in our study is similar to the range of values measured for expressed $Ca_V3.2$ but more than 20-fold lower than $Ca_V3.1$ (Lee et al., 1999; Jeong et al., 2003; Perez-Reyes, 2003; Kang et al., 2006), the other major subunit known to be expressed in heart (Perez-Reyes, 2003; Vassort et al., 2006).

Na^+ Channel Toxins Interact with T-Type Ca^{2+} Channels

The most salient observation of the present study was the demonstration that TTX and STX interact with I_{CaT}. The nature of the TTX interaction is very peculiar in that the toxin does not apparently influence the voltage dependence and kinetics of cardiac I_{CaT} but reduces the efficacy of Ni^{2+}-induced block of this current. With the exception of $Ca_V3.3$, which was blocked by TTX, the toxin produced similar effects on I_{CaT} arising from $Ca_V3.1$ or $Ca_V3.2$ expressed in HEK-293 cells. It appears unlikely that the effects of both toxins would be due to the presence of undesired contaminants as suggested by Jones and Marks (1989), who reported that STX produced a variable inhibition of a low threshold Ca^{2+} current in bullfrog sympathetic neurons whose potency varied with different batches of the toxin. We tested TTX and STX from respectively two and three different commercial sources and obtained results that were quantitatively similar. The responses of I_{CaT} to both toxins were also unaffected by buffering heavy metals with EDTA, arguing against the possibility that such metals significantly contaminate the commercial toxin preparations.

Although it has been suggested that part of the inhibitory activity of Ni^{2+} takes place in the pore region between S5 and S6 (Lee et al., 1999), a more recent study from the same group postulated that His191 of $Ca_V3.2$, as opposed to Gln172 in $Ca_V3.1$ located in the extracellular loop between S3 and S4 of domain I, is responsible for the ∼60-fold higher sensitivity of this channel to Ni^{2+} than $Ca_V3.1$ (Kang et al., 2006). In view of the location of this site in close proximity to the voltage sensor in S4 and its remote location from the P-loop, combined with the fact that the block by Ni^{2+} was use independent, Kang et al. (2006) proposed that the divalent cation exerts its inhibitory activity by an effect on gating resulting in pore closure. Whether TTX is able to bind to this site is unknown. However, our data clearly showed that TTX competitively antagonized without mimicking the effect of Ni^{2+} on native I_{CaT}, an effect that was also observed with $Ca_V3.1$ and $Ca_V3.2$. Such an interaction could potentially explain why the toxin did not exert any effect on native or these cloned I_{CaT} in the absence of the blocker. In this scheme, STX would not only bind to the same site with higher affinity, presumably facilitated by its additional positive charge, but would also imitate Ni^{2+} by mediating block of the pore. However, histidine at that same position is also replaced by a glutamine (Gln172) in $Ca_V3.3$ and yet STX blocked $Ca_V3.2$ and $Ca_V3.3$ with nearly equal efficacies, and TTX also blocked this current.

An alternative hypothesis is that TTX binds to, as it does on Na^+ channels, a region within the outer vestibule near the pore of I_{CaT} channels. TTX binding would not obstruct Ca^{2+} binding and flux through the pore but would partially occlude the binding of Ni^{2+} through a competitive interaction, or alternatively by a remote alteration of the structure of the Ni^{2+} binding site between S3 and S4 of domain I (His191) when the toxin occupies the pore. On the other hand, STX would bind these channels with higher affinity than TTX, perhaps due to the presence of an additional positively charged guanidinium group, resulting in reduced Ca^{2+} entry through the pore. The alignment of the pore region of the four domains of several Na^+ channel subtypes and $Ca_V3.1$, $Ca_V3.2$, and $Ca_V3.3$ is displayed in Fig. 1. The figure highlights in red the critical residues reported to be involved in TTX and STX binding (Terlau et al., 1991). Based on the results of single point mutations, the amino acids of the four repeat domains forming the SF of Na^+ channels (0') and those downstream from the N terminus by four positions (3′) are postulated to form two rings of charges that are critical for toxin interaction with the pore (Terlau et al., 1991; Hille, 2001). Lipkind and Fozzard (1994) performed molecular modeling of the interaction of TTX with the rat brain II and skeletal muscle ($Na_V1.4$) Na^+ channels, which are sensitive

to TTX in the nanomolar range, and suggested that the positive charge of the guanidinium group of TTX interacts electrostatically with three carboxyl groups of Domains I (D384, E387) and II (E942), while the hydroxyl groups of C10 and C11 of TTX would form hydrogen bonds with Glu 945 of Domain II. It has been demonstrated that the aromatic residue Tyr or Phe of TTX-sensitive channels located immediately adjacent to Asp 384 of Domain I is responsible for conferring high sensitivity of these Na^+ channels to the toxin. This residue is substituted by a cysteine in the cardiac-specific TTX-resistant isoform $Na_V1.5$ (Backx et al., 1992; Satin et al., 1992; Fig. 1) or by a Ser in the TTX-insensitive Na^+ channels found in the nervous system ($Na_V1.8$ and $Na_V1.9$; Fig. 1). The cysteine at that position is also responsible for the higher sensitivity of the cardiac-type Na^+ channel to group IIb metals such as Cd^{2+} and Zn^{2+} (Satin et al., 1992; Backx et al., 1992). The model of Lipkind and Fozzard (1994) was also able to predict the important role played by the aromatic residue that stabilized toxin binding most likely by an interaction with its ring structure. It was predicted that due to the presence of a second guanidinium group, the additional positive charge would also interact with Asp 1717 of Domains IV. In a subsequent study examining differences in interactions of the two toxins, Penzotti et al. (1998) showed that while mutations of the selectivity residues (DEKA) produced equivalent effects on both toxins, the aromatic residue (C, Y, or F) adjacent to the Asp (D400 of $Na_V1.4$; Fig. 1) of Domain I involved in selectivity is more important for TTX binding, while the outer residues of Domains II (E758 of $Na_V1.4$) and IV (D1540 of $Na_V1.4$) play a more critical function in STX binding. Using various analogues of STX, Choudhary et al. (2002) confirmed the critical role of the outer vestibular Asp1539 of Domain IV (Fig. 1) for the interaction of C11 of STX with $Na_V1.4$. A more recent study revisited the possibility of an interaction of TTX with the same residue of Domain IV (Choudhary et al., 2003). The study showed that the hydroxyl group at C11 of TTX probably interacts through hydrogen bonding with the outer vestibular Asp residue of Domain IV (Choudhary et al., 2003). According to this model, the guanidinium group of TTX would interact with the selectivity filter, and the toxin would be docked tilted across the outer vestibule stabilized by hydrogen bonds between C10 and Glu403 of Domain I, and C11 with Asp1539 of Domain IV. When comparing the pore residues of $Ca_V3.1$–$Ca_V3.3$ with mammalian TTX-sensitive ($Na_V1.4$) and TTX-insensitive ($Na_V1.5$, $Na_V1.8$ and $Na_V1.9$) Na^+ channels (Fig. 1), although many identical amino acids as well as equivalent substitutions can be identified, in particular the residues involved in channel selectivity (SF in Fig. 1) and toxin binding, all outer ring residues critical for TTX and STX binding to Na^+ are replaced by either neutral, hydrophobic, or positively charged amino acids in T-type Ca^{2+} channels. This could form the basis for the reduced apparent affinity of STX for native and cloned T-type Ca^{2+} channels. However, this scheme would be difficult to reconcile with the lack of effect of TTX on native and two of the Ca_V3 channels since binding of TTX to the selectivity filter residues Glu and Asp would be expected to alter ion permeation, which was not observed, as both native and $Ca_V3.1$ and $Ca_V3.2$-mediated T-type Ca^{2+} channels were unaffected by TTX in the absence of Ni^{2+}. The fact that TTX blocks $Ca_V3.3$ but not $Ca_V3.1$ and $Ca_V3.2$ is difficult to explain on the basis of the primary amino acid sequence forming the pores as they are nearly identical with the exception perhaps of a neutral Gln (identified in black in Fig. 1) replacing the positively charged Arg at $-5'$ position from the selectivity filter of Domain IV. Interestingly, this Gln residue is also present in the TTX-insensitive mammalian Na^+ channels ($Na_V1.5$, $Na_V1.8$, and $Na_V1.9$). Clearly a thorough mutational analysis will be necessary to determine the possible contribution of His191 between S3 and S4 of Domain I and that of P-loop residues of all domains in the binding of Na^+ channel toxins to T-type Ca^{2+} channels.

Evolutionary Properties of Na^+ and T-type Ca^{2+} Channels

Voltage-dependent Na^+ and Ca^{2+} channels have been hypothesized to have evolved from a common ancestor (Hille, 2001). This hypothesis is supported by comparing the sequences of cloned Na^+ and T-type Ca^{2+} channels and their respective functional properties. Our data further extend this hypothesis by providing evidence that Na^+ channel toxins also interact with native cardiac and cloned T-type Ca^{2+} channels. A link between the structure of the pore and the gating of $Ca_V3.1$ has recently been established (Talavera et al., 2003). Divalent cations compete with TTX and STX for common binding sites along the inner pore of Na^+ channels (Doyle et al., 1993), which is similar to the rightward shift by TTX of the dose–response relationship of the Ni^{2+}-induced block of native I_{CaT} and the attenuated block by Ni^{2+} of $Ca_V3.1$ and $Ca_V3.2$ expressed in HEK-293 cells. Geffeney et al. (2005) analyzed the Na^+ channel pore residues involved in the lack of sensitivity to TTX of skeletal muscle Na^+ channels of different populations of garter snake that have coevolved with toxic newt preys in California, Oregon, and Idaho. For these particular Na^+ channels, all of the "classical" residues in Domains I, II, and III involved in the TTX sensitivity of mammalian Na^+ channels were identical to those of highly TTX-sensitive Na^+ channels (e.g., $Na_V1.4$ in Fig. 1) and were thus excluded to explain their TTX insensitivity. Analysis of four different populations of snake identified two major residues in the P-loop of Domain IV, Asn for Asp at position $+3'$, and Val for Iso at position $-4'$, from the selectivity filter. Geffeney et al. (2005) found this double mutation (and an additional less important one) in the Willow Creek garter snake Na^+

channel to be of prime importance in conferring extremely poor sensitivity to TTX compared with Na^+ channels of other snakes. Curiously, these two identical substitutions are also found in the three T-type Ca^{2+} channel clones (Fig. 1). Site-directed mutagenesis experiments of these two sites and adjacent sites (e.g., Gln at $-5'$ position of the selectivity filter in Domain IV of $Ca_V3.3$) combined with structural modeling of the pore should enable us to determine if they reflect pure coincidences or whether they bear any evolutionary foundation pointing toward an ancestral TTX-insensitive voltage-gated cation channel.

We thank Dr. A. Beedle for providing the $hCa_V3.1$ cDNA, NeuroMed Pharmaceuticals for $hCa_V3.2$, and Dr. A. Monteil for $hCa_V3.3$.

This study was supported by grants awarded to N. Leblanc, G. W. Zamponi, and S. Nattel from the Canadian Institutes of Health Research, the Québec Heart and Stroke Foundation (HSF), and The Montréal Heart Institute Fund, and from grants to N. Leblanc from the National Institutes of Health (NIH) (grant HL 1 R01 HL075477) and the Max Baer Heart Fund. This publication was also made possible by grant NCRR 5P20 RR15581 (N. Leblanc) from the National Center for Research Resources (NCRR), a component of the NIH supporting a Center of Biomedical Research Excellence at the University of Nevada School of Medicine (Reno, NV). G.W. Zamponi is a Scientist of the Alberta Heritage Foundation for Medical Research (AHFMR) and a Canada Research Chair. D. Varela holds fellowship awards from the AHFMR and the HSF. The contents of the manuscript are solely the responsibility of the authors and do not necessarily represent the official views of NCRR or NIH.

Angus C. Nairn served as editor.

Submitted: 14 September 2007
Accepted: 22 May 2008

REFERENCES

Aggarwal, R., S.R. Shorofsky, L. Goldman, and C.W. Balke. 1997. Tetrodotoxin-blockable calcium currents in rat ventricular myocytes; a third type of cardiac cell sodium current. *J. Physiol.* 505:353–369.

Alvarez, J.L., E. Salinas-Stefanon, G. Orta, T. Ferrer, K. Talavera, L. Galan, and G. Vassort. 2004. Occurrence of a tetrodotoxin-sensitive calcium current in rat ventricular myocytes after long-term myocardial infarction. *Cardiovasc. Res.* 63:653–661.

Backx, P.H., D.T. Yue, J.H. Lawrence, E. Marban, and G.F. Tomaselli. 1992. Molecular localization of an ion-binding site within the pore of mammalian sodium channels. *Science.* 257:248–251.

Bean, B.P. 1985. Two kinds of calcium channels in canine atrial cells. Differences in kinetics, selectivity, and pharmacology. *J. Gen. Physiol.* 86:1–30.

Catterall, W.A. 2000. From ionic currents to molecular mechanisms: the structure and function of voltage-gated sodium channels. *Neuron.* 26:13–25.

Choudhary, G., L. Shang, X. Li, and S.C. Dudley Jr. 2002. Energetic localization of saxitoxin in its channel binding site. *Biophys. J.* 83:912–919.

Choudhary, G., M. Yotsu-Yamashita, L. Shang, T. Yasumoto, and S.C. Dudley. 2003. Interactions of the C-11 hydroxyl of tetrodotoxin with the sodium channel outer vestibule. *Biophys. J.* 84:287–294.

Cole, W.C., D. Chartier, M. Martin, and N. Leblanc. 1997. Ca^{2+} permeation through Na^+ channels in guinea pig ventricular myocytes. *Am. J. Physiol.* 273:H128–H137.

Cribbs, L.L., J.H. Lee, J. Yang, J. Satin, Y. Zhang, A. Daud, J. Barclay, M.P. Williamson, M. Fox, M. Rees, and E. PerezReyes. 1998. Cloning and characterization of α_{1H} from human heart, a member of the T-type Ca^{2+} channel gene family. *Circ. Res.* 83:103–109.

Cribbs, L.L., B.L. Martin, E.A. Schroder, B.B. Keller, B.P. Delisle, and J. Satin. 2001. Identification of the T-type calcium channel ($Ca_V3.1d$) in developing mouse heart. *Circ. Res.* 88:403–407.

Doyle, D.D., Y. Guo, S.L. Lustig, J. Satin, R.B. Rogart, and H.A. Fozzard. 1993. Divalent cation competition with ^{H3}saxitoxin binding to tetrodotoxin-resistant and tetrodotoxin-sensitive sodium channels—a two-site structural model of ion/toxin interaction. *J. Gen. Physiol.* 101:153–182.

Fareh, S., A. Benardeau, and S. Nattel. 2001. Differential efficacy of L- and T-type calcium channel blockers in preventing tachycardia-induced atrial remodeling in dogs. *Cardiovasc. Res.* 49:762–770.

Geffeney, S.L., E. Fujimoto, E.D. Brodie III, E.D. Brodie Jr., and P.C. Ruben. 2005. Evolutionary diversification of TTX-resistant sodium channels in a predator-prey interaction. *Nature.* 434:759–763.

Han, W., W. Bao, Z. Wang, and S. Nattel. 2002. Comparison of ion-channel subunit expression in canine cardiac Purkinje fibers and ventricular muscle. *Circ. Res.* 91:790–797.

Heinemann, S.H., H. Teriau, W. Stuhmer, K. Imoto, and S. Numa. 1992. Calcium channel characteristics conferred on the sodium channel by single mutations. *Nature.* 356:441–443.

Heubach, J.F., A. Kohler, E. Wettwer, and U. Ravens. 2000. T-type and tetrodotoxin-sensitive Ca^{2+} currents coexist in guinea pig ventricular myocytes and are both blocked by mibefradil. *Circ. Res.* 86:628–635.

Hille, B. 2001. Ion Channels of Excitable Membranes. Third edition. Sinauer Associates, Inc., Sunderland, MA. 814 pp.

Hobai, I.A., J.C. Hancox, and A.J. Levi. 2000. Inhibition by nickel of the L-type Ca channel in guinea pig ventricular myocytes and effect of internal cAMP. *Am. J. Physiol. Heart Circ. Physiol.* 279:H692–H701.

Jeong, S.W., B.G. Park, J.Y. Park, J.W. Lee, and J.H. Lee. 2003. Divalent metals differentially block cloned T-type calcium channels. *Neuroreport.* 14:1537–1540.

Jones, S.W., and T.N. Marks. 1989. Calcium currents in bullfrog sympathetic neurons. I. Activation kinetics and pharmacology. *J. Gen. Physiol.* 94:151–167.

Kang, H.W., J.Y. Park, S.W. Jeong, J.A. Kim, H.J. Moon, E. Perez-Reyes, and J.H. Lee. 2006. A molecular determinant of nickel inhibition in Cav3.2 T-type calcium channels. *J. Biol. Chem.* 281:4823–4830.

Lee, J.H., J.C. Gomora, L.L. Cribbs, and E. Perez-Reyes. 1999. Nickel block of three cloned T-type calcium channels: low concentrations selectively block α_{1H}. *Biophys. J.* 77:3034–3042.

Lemaire, S., C. Piot, J. Seguin, J. Nargeot, and S. Richard. 1995. Tetrodotoxin-sensitive Ca^{2+} and Ba^{2+} currents in human atrial cells. *Receptors Channels.* 3:71–81.

Lipkind, G.M., and H.A. Fozzard. 1994. A structural model of the tetrodotoxin and saxitoxin binding site of the Na^+ channel. *Biophys. J.* 66:1–13.

McDonald, T.F., S. Pelzer, W. Trautwein, and D.J. Pelzer. 1994. Regulation and modulation of calcium channels in cardiac, skeletal, and smooth muscle cells. *Physiol. Rev.* 74:365–507.

McNulty, M.M., J.W. Kyle, G.M. Lipkind, and D.A. Hanck. 2006. An inner pore residue (Asn406) in the Nav1.5 channel controls slow inactivation and enhances mibefradil block to T-type Ca^{2+} channel levels. *Mol. Pharmacol.* 70:1514–1523.

Mitra, R., and M. Morad. 1986. Two types of calcium channels in guinea pig ventricular myocytes. *Proc. Natl. Acad. Sci. USA.* 83:5340–5344.

Monteil, A., J. Chemin, E. Bourinet, G. Mennessier, P. Lory, and J. Nargeot. 2000. Molecular and functional properties of the human α_{1G} subunit that forms T-type calcium channels. *J. Biol. Chem.* 275:6090–6100.

Penzotti, J.L., H.A. Fozzard, G.M. Lipkind, and S.C. Dudley Jr. 1998. Differences in saxitoxin and tetrodotoxin binding revealed by mutagenesis of the Na^+ channel outer vestibule. *Biophys. J.* 75:2647–2657.

Perez-Reyes, E. 2003. Molecular physiology of low-voltage-activated T-type calcium channels. *Physiol. Rev.* 83:117–161.

Santana, L.F., A.M. Gomez, and W.J. Lederer. 1998. Ca^{2+} flux through promiscuous cardiac Na^+ channels: slip-mode conductance. *Science.* 279:1027–1033.

Satin, J., and L.L. Cribbs. 2000. Identification of a T-type Ca^{2+} channel isoform in murine atrial myocytes (AT-1 cells). *Circ. Res.* 86:636–642.

Satin, J., J.W. Kyle, M. Chen, P. Bell, L.L. Cribbs, H.A. Fozzard, and R.B. Rogart. 1992. A mutant of TTX-resistant cardiac sodium channels with TTX-sensitive properties. *Science.* 256:1202–1205.

Sha, Q., S.W. Robinson, S.L. McCulle, S.R. Shorofsky, P.A. Welling, L. Goldman, and C.W. Balke. 2003. An antisense oligonucleotide against H1 inhibits the classical sodium current but not $I_{Ca(TTX)}$ in rat ventricular cells. *J. Physiol.* 547:435–440.

Strong, M., and G.A. Gutman. 1993. Missing link in ion channels. *Nature.* 362:26.

Su, Z., M. Sheets, H. Ishida, F. Li, and W.H. Barry. 2004. Saxitoxin blocks L-type I_{Ca}. *J. Pharmacol. Exp. Ther.* 308:324–329.

Talavera, K., A. Janssens, N. Klugbauer, G. Droogmans, and B. Nilius. 2003. Pore structure influences gating properties of the T-type Ca^{2+} channel α_{1G}. *J. Gen. Physiol.* 121:529–540.

Terlau, H., S.H. Heinemann, W. Stuhmer, M. Pusch, F. Conti, K. Imoto, and S. Numa. 1991. Mapping the site of block by tetrodotoxin and saxitoxin of sodium channel II. *FEBS Lett.* 293:93–96.

Vassort, G., K. Talavera, and J.L. Alvarez. 2006. Role of T-type Ca^{2+} channels in the heart. *Cell Calcium.* 40:205–220.

Zhang, Y., L.L. Cribbs, and J. Satin. 2000. Arachidonic acid modulation of α_{1H}, a cloned human T-type calcium channel. *Am. J. Physiol. Heart Circ. Physiol.* 278:H184–H193.